

Theoretical Study on Acylacetanilide Azomethine Dyes: A Relationship between Electronic Absorption Properties and Molecular Structures

Seiji Ichijima* **and Hidetoshi Kobayashi**[1]

Analysis Technology Center, Advanced Core Technology Laboratories, Research & Development Management Headquarters, Fuji Photo Film Co., Ltd., Minamiashigara, Kanagawa 250-0193

[1]Research & Development Management Headquarters, Fuji Photo Film Co., Ltd., Minato-ku, Tokyo 106-8620

Received February 9, 2005; E-mail: seiji_ichijima@fujifilm.co.jp

The relationship between visual absorption properties and molecular structures was investigated for a series of yellow azomethine dyes derived from 4-diethylamino-2-methylaniline and 2-acyl-2′-chloroacetanilides, in which the acyl groups are 1-indolinylcarbonyl (IA), 1-methylcyclopropylcarbonyl (CA), acetyl, benzoyl, and pivaloyl (PA). DFT calculations predicted major conformational isomers attributed to deviations from the planarity of the *p*-aminophenyl–azomethine fragment. Observed wavelengths were well reproduced by TD-DFT calculations at global minimum geometries, whereas the intensities correlate with the Boltzmann-weighted oscillator strengths. The observed intensities varied by 1.5 times from minimum to maximum without significant shifts in the peak wavelengths, demonstrating the largest absorption of IA and the distinct increase of absorption by changing the acyl group from open- (PA) to closed-ring (CA). The different acyl groups nearly perpendicular to the azomethine fragment in global minima alter frontier orbital energies, while leaving HOMO–LUMO energy gaps almost unchanged. The acyl groups, which are twisted largely in local minima, exert mesomeric effects to lower the LUMO energies. The planarity of the *p*-aminophenyl–azomethine fragment affects HOMO–LUMO overlapping, but hardly changes HOMO and LUMO energies. These electronic and steric effects rationalize the absorption intensities and peak wavelengths observed for the dyes and also the sharp-cut curves of spectra in the long-wavelength sides for IA and CA.

Azomethine dyes are known to be among the most important dyes because of their wide applications, including color photographic systems, dye diffusion thermal transfer (D2T2) print systems, and others.[1] Due to their central roles as image dyes, they have been the subjects of considerable research interest in order to understand their spectral and photophysical properties. To elucidate the absorption properties of azomethine dyes, theoretical calculations on geometry as well as absorption properties are of crucial importance because of their flexibility in geometry and the strong dependence of absorption properties on it.

In color photographic systems, yellow azomethine dyes are formed during the developing process by the oxidative coupling reactions of 4-dialkylaminoanilines with 2-acylacetanilides coated on film. To realize good color reproducibility, it is necessary that the absorption spectrum of a yellow dye has a sharp-cut curve in the long-wavelength side. In addition, as the extinction coefficient in the blue absorption band for a yellow dye increases, the light-sensitive layer coated on a film can be thinned by reducing the amount of 2-acylacetanilide required to produce a given density. As a result, undesired image smear caused by light scattering is decreased, and the optical image becomes sharper.

Tailoring the azomethine dye molecule to achieve optimal dye properties has been a formidable task since the pioneering work by Brown et al.[2] about 40 years ago. Several theoretical and experimental investigations on the structures and the absorption spectra of azomethine dyes have been performed over the past decade. Nakamura et al.[3] examined the torsion dependence of the absorption spectra for indoaniline dyes, which are widely used as cyan image dyes. Using the structures obtained by both X-ray crystal structure analysis and molecular orbital (MO) calculations with the AM1 method,[4] the absorption wavelengths and their intensities were calculated by the INDO/S method.[5] It is stated that a decrease in the degree of planarity brings about a red shift and a lowering of the absorption intensity in the longest transition. Friedrich et al.[6] compared the structures and the absorption wavelengths calculated for azomethine dyes with several semi-empirical MO methods. They reported that the AM1 method predicts the bond lengths and the bond angles within statistical error, but gives incorrect torsion angles for flexible molecules, such as 2-acylacetanilide azomethine dyes. In addition, it is reported that the INDO/S method is the most useful for evaluating the absorption wavelengths among the semi-empirical MO methods, when an accurate geometry of the dye is given. We determined the molecular structures crystallographically for several 2-acylacetanilide azomethine dyes.[7] In the molecular structures, the *p*-aminophenyl fragment is coplanar with the azomethine–carbamoyl fragment, but perpendicular to the acyl group. Daiba et al.[8] examined the molar extinction coefficients of 2-acylacetanilide azomethine dyes. Using the structures obtained by combining the Monte-Carlo method and molecular orbital calculations at the AM1 level, the absorption wavelengths and their intensities were calculated by the INDO/S method. Abu-Hasanayn et al.[9] carried out geometry optimiza-

Published on the web October 31, 2005; DOI 10.1246/bcsj.78.1929

tion for some 2-acylacetanilide azomethine dyes both in the ground state and in the lowest triplet state.

While ab initio quantum chemistry has recently developed into a powerful tool for studying both geometries and electronic absorption properties, its routine use often encounters at least two difficulties: high computational cost and the choice of the theoretical levels. The need to include quantitative descriptions of the photophysical properties calls for balanced and accurate descriptions of ground and excited states with accurate geometries. Therefore, it is mandatory for satisfactory evaluations to use quantum chemical methods that include the effects of dynamic electron correlation. Among the correlated methods, the density functional theory (DFT) method[10] has successfully led to the combination of low computational cost with reasonable accuracy for the prediction of molecular geometries and energies in minimum states. It is also known that the time-dependent density functional theory (TD-DFT) method has been successfully applied to treat excited-state properties,[11] although it has only recently been applied to medium-size dye molecules,[12] more than 20 years after it was first proposed.[13]

In this context, we recently examined the stable geometries and the spectroscopic properties of the azomethine dyes derived from benzoylacetanilide (BA) and pivaloylacetanilide (PA) (Fig. 1), of which types of dyes have long been used in modern photographic films as yellow-image dyes, both experimentally and theoretically.[14] Using DFT and TD-DFT methods, we revealed that the absorption intensity is dominated by both the planarity between *p*-aminophenyl and azomethine–carbamoyl fragments and the orthogonality between acyl group and azomethine–carbamoyl fragment. It is also reported that the sharp-cut curve of a spectrum in the long-wavelength side observed for PA is due to a low population of its conformational isomer unlike the case of BA.

In this article, aiming at a more complete understanding of the stable geometries and absorption properties, we examine a series of 2-acylacetanilide azomethine dyes, shown in Fig. 1, using the DFT and TD-DFT methods. We also elucidate the reason that dyes, in which the acyl groups are 1-indolinylcarbonyl (IA)[15] and 1-methylcyclopropylcarbonyl (CA),[16] show high absorption intensities of the band in the blue region and sharp-cut curves in the long-wavelength sides of absorption spectra compared with the other dyes. Although not directly relevant to this study, we note in passing that IA and CA types of dyes with optimized substituents have been used during the past decade in reversal[17] and negative[7b] films, respectively.

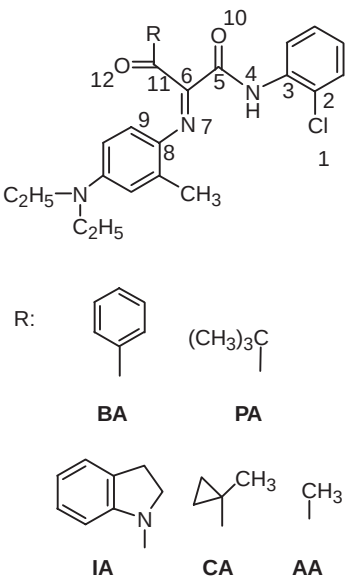

Fig. 1. Chemical structures and labeling of the dyes investigated. Numerical values indicate the atom numbering.

Method

Materials. Using the procedure reported by Brown et al.,[2] azomethine dyes were synthesized by the oxidative coupling reactions of 4-diethylamino-2-methylaniline with 2-acyl-2′-chloroacetanilides, in which ammonium peroxodisulfate was used as the oxidizing agent. We used 2-acylacetanilides with a so-called "ballast" group because of high solubility of the dyes in organic solvents. Figure 2 shows the chemical structures of the dyes with a ballast group. In color photographic systems, a ballast group is attached to anchor the 2-acylacetanilide in the appropriate layer, to prevent its dye from wandering into adjacent layers, and to enable 2-acylacetanilide and the dye to be highly soluble in organic solvents. As shown in Fig. 2, the ballasting substituent that we used here, which consists of a combination of aliphatic and aromatic groups, is widely known in the field of color photographic systems.[1b]

Measurement of the Absorption Spectra. The dyes shown in Fig. 2 were diluted with ethyl acetate in the spectrum grade, made by Wako Chemical Co., Ltd., to prepare solution samples of 1×10^{-3} M ($1\,\mathrm{M} = 1\ \mathrm{mol\,dm^{-3}}$), respectively. The visible absorption spectra of the samples were recorded with a 1 mm cell using a Shimadzu Automatic Recording Spectrophotometer (UV260).

Molecular Orbital Calculations. Figure 1 shows the chemical structures for calculations and labeling of the dyes. Numerical values indicate the atom numbering. To obtain the stable geometries of the dyes, we performed calculations at the level of the DFT method with the Becke's nonlocal three-parameter hybrid exchange functional (B3)[18] in conjunction with the Lee–Yang–Parr correlation functional (LYP)[19] with the polarized split-valence shell 6-31G(d) basis set (B3LYP/6-31G(d)).[20] Consistent with the previous investigation,[14] the geometries of stationary points were located on the potential energy curves for the rotation of *p*-aminophenyl, acyl, and carbamoyl fragments. At the optimized geometries, vibrational analyses were performed to ensure that the stationary points found do not have imaginary frequencies. To calculate more accurate energy differences between conformers, we

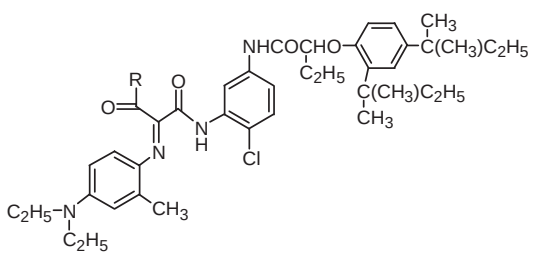

Fig. 2. Chemical structures of the dyes with a ballast group. R denotes the same meaning as that shown in Fig. 1.

performed single-point energy calculations with additional diffuse functions (B3LYP/6-31+G(d)), using the optimized geometries obtained for the dyes at the B3LYP/6-31G(d) level. The computed frequencies calculated at the B3LYP/6-31G(d) level were used to estimate the zero-point energy (ZPE) corrections with a scaling factor of 0.9806.[21]

Furthermore, using the optimized geometries obtained for the dyes with the B3LYP/6-31G(d) method, lower energy vertical excitations and their corresponding intensities were calculated with the time-dependent density functional theory (TD-DFT) method using the B3LYP functional with the 6-31G(d) and 6-31+G(d) basis sets. All of the above-mentioned calculations were performed using the Gaussian 98[22] package.

Results

Structural Features. Figure 3 shows the minimum energy conformations of IA, CA, and AA obtained at the B3LYP/6-31G(d) level calculations. To distinguish between conformations, the same labeling (MS number) is used for analogs of conformations. For a series of the dyes, we found MS1 and MS2 types of conformers attributed to deviations from planarity of *p*-aminophenyl–azomethine fragments consistent with the global and local minimum conformations, respectively, for BA and PA obtained at the same calculation level in our previous report.[14] Schematic Newman projections of MS1 and MS2 conformations along the C(6)–(C11) bond are shown in Fig. 4, accounting for conformational isomers in common

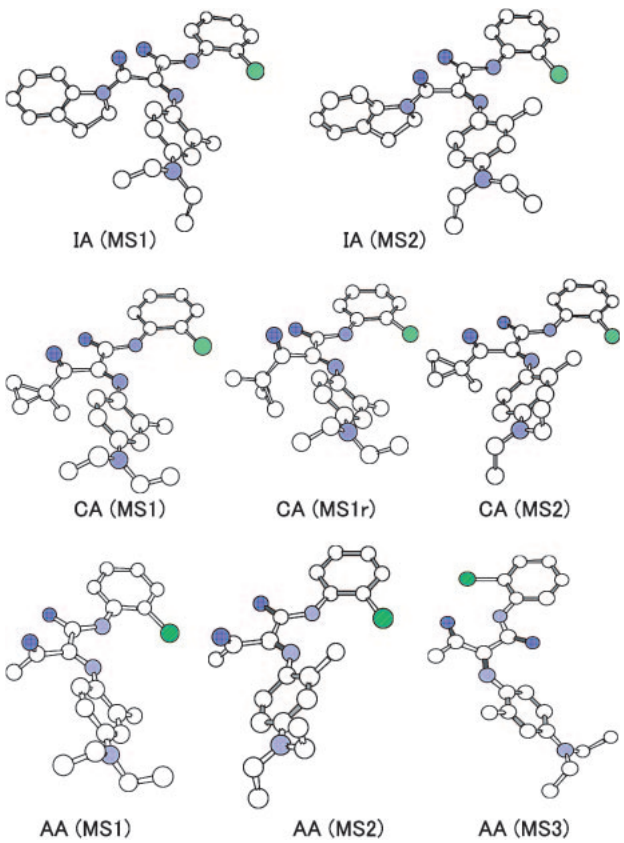

Fig. 3. Calculated minimum energy conformations and their labeling of the conformations in parenthesis for IA, CA, and AA. Hydrogen atoms are not shown.

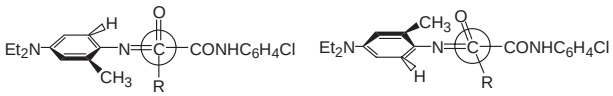

Fig. 4. Schematic Newman projections of MS1 and MS2 conformations for the dyes along the C(6)–(C11) bond.

for 2-acylacetanilide azomethine dyes. In addition to them, we found the minimum energy conformations for CA and AA: MS1r for CA is the rotamer of MS1 around the bond between 1-methylcyclopropyl and carbonyl groups, and MS3 for AA is the nearly planar conformation. No equilibrium geometries of the rotamer of MS1r attributed to the deviation from planarity of the *p*-aminophenyl–azomethine fragment were found.

Table 1 presents the geometrical parameters of the equilibrium geometries obtained at the B3LYP/6-31G(d) level. The torsion angles of t1–t6 are defined for ∠C2–C3–N4–C5, ∠C3–N4–C5–C6, ∠N4–C5–C6–N7, ∠C5–C6–N7–C8, ∠C6–N7–C8–C9, and ∠N7–C6–C11–O12, respectively, as indicated in Table 1. Those of t1–t4 in any dye are calculated around 0° or 180° for MS1, MS1r, and MS2 conformations, indicating the same high planarity of the azomethine–carbamoyl fragments. The opposite signs of torsion angle t5 for MS1 and MS2 are responsible for the opposite twist direction of the *p*-aminophenyl fragment from azomethine–carbamoyl fragments, as seen in Fig. 4. The change in torsion angle t5 for MS2 between the dyes is larger than that for MS1 (36.3–23.0° vs −36.1–−29.1°), and in any dye the deviation of t6 from 90° for MS2 is larger than that for MS1. It should be noted that the spatial relation in MS2 between the acyl R group and the *p*-aminophenyl fragment varies depending on the acyl R group, whereas that in MS1 between the acyl oxygen atom and the *p*-aminophenyl fragment is identical among the dyes. Therefore, the geometry variation of MS1 among the dyes is relatively small. The prominent changes in bond lengths between the conformers are found in AA; the shorter C(6)–C(11) and N(7)–C(8) bonds and the longer C(5)–C(6) and C(11)–O(12) bonds are calculated for MS3 compared to the corresponding bonds for the other conformers, indicating a π-conjugation of the *p*-aminophenyl–azomethine fragment extending to the acetyl group. In addition, the strong hydrogen bond of O(12)···HN(4) can be recognized. This MS3 conformation is energetically accessible only for AA because of the small acyl group (vide infra).

Table 2 gives the calculated energies (ΔE) with and without ZPE corrections and Boltzmann distributions relative to the global minima for the dyes investigated. In all cases, MS1 conformations correspond to the global minima, but in a comparison of the B3LYP/6-31G(d) relative energies and the B3LYP/6-31+G(d) single-point relative energies, the basis set dependence is evident in the significant difference in results calculated with MS3 for AA; it alters the energetic order of MS2 and MS3. It is likely due to the more accurate prediction of energy that the calculation with an additional set of diffuse functions gives a higher relative energy than that without diffuse functions for MS3 in AA, which is the geometry with a strong hydrogen bond. Similar effects have been reported in

Table 1. Selected Geometrical Parameters in the Structures Obtained by DFT Calculations and the Definition of Torsion Angles of t1–t6

Geometrical parameters	BA[a]		PA[a]		IA		CA			AA		
	MS1	MS2	MS1	MS2	MS1	MS2	MS1	MS1r	MS2	MS1	MS2	MS3
Bond length/Å												
N4–C5	1.370	1.371	1.367	1.368	1.369	1.370	1.369	1.370	1.369	1.368	1.369	1.373
C5–O10	1.228	1.229	1.231	1.231	1.230	1.231	1.230	1.229	1.231	1.231	1.231	1.228
C5–C6	1.509	1.508	1.508	1.512	1.509	1.508	1.508	1.511	1.507	1.509	1.510	1.528
C6–N7	1.283	1.285	1.282	1.284	1.284	1.286	1.283	1.285	1.284	1.284	1.285	1.296
C6–C11	1.532	1.534	1.537	1.544	1.528	1.529	1.533	1.536	1.534	1.533	1.534	1.504
N7–C8	1.397	1.394	1.398	1.394	1.395	1.393	1.398	1.397	1.395	1.396	1.393	1.376
C11–O12	1.222	1.220	1.217	1.216	1.229	1.226	1.222	1.222	1.220	1.216	1.215	1.231
Hydrogen bond length/Å												
Cl1–HN4	2.488	2.492	2.488	2.486	2.488	2.497	2.490	2.489	2.491	2.488	2.489	2.498
N7(or O12)–HN4	2.166	2.162	2.159	2.123	2.170	2.157	2.170	2.157	2.159	2.161	2.143	1.838
Bond angle/°												
C5–C6–N7	118.8	118.5	118.4	117.1	118.5	118.3	118.7	118.2	118.5	118.5	118.0	125.1
C5–C6–C11	112.9	113.4	112.7	115.5	113.2	114.1	112.5	113.6	113.4	113.0	114.5	121.1
N7–C6–C11	128.3	127.6	128.8	126.6	128.2	126.9	128.8	128.1	127.6	128.4	127.2	113.6
C6–N7–C8	127.2	127.1	127.8	127.2	128.2	127.7	127.8	127.8	127.0	128.2	127.3	131.5
Torsion angle/°												
t1: C2–C3–N4–C5	−178.8	−179.6	−178.9	−179.2	−178.8	−176.9	−178.8	−178.7	−178.7	−180.0	−178.7	175.7
t2: C3–N4–C5–C6	178.7	−179.0	179.1	−178.8	178.8	179.7	178.9	178.7	−179.3	−179.7	−178.8	179.0
t3: N4–C5–C6–N7	−5.2	3.9	−6.0	6.0	−9.1	1.2	−7.0	−7.7	2.1	−4.4	3.7	162.0
t4: C5–C6–N7–C8	178.7	−178.7	178.6	−179.2	−180.0	−179.6	179.6	177.8	−178.4	178.4	−177.4	−16.0
t5: C6–N7–C8–C9	−34.2	28.0	−36.1	36.3	−29.0	23.0	−33.6	−31.0	27.7	−35.5	29.4	−27.6
t6: N7–C6–C11–O12	91.3	67.0	84.3	58.8	84.2	67.5	85.4	92.3	67.9	78.0	59.7	−166.1

a) From Ref. 14.

Table 2. Energies (ΔE)[a] and Boltzmann Distribution (BD)[b] Relative to Global Minima (MS1) for Conformers

Compd	Geometry	B3LYP/6-31G(d)		B3LYP/6-31+G(d)[c]	
		ΔE	BD	ΔE	BD
BA	MS2	1.55 (1.69[d])	0.53	0.88 (1.02)	0.70
PA	MS2	8.23 (8.20[d])	0.04	7.13 (7.10)	0.06
IA	MS2	3.28 (3.78)	0.27	5.26 (5.76)	0.12
CA	MS1r	2.05 (2.28)	0.44	1.38 (1.61)	0.57
	MS2	1.89 (1.94)	0.47	1.81 (1.86)	0.48
AA	MS2	2.96 (3.47)	0.30	2.25 (2.76)	0.40
	MS3	2.32 (0.86)	0.39	4.74 (3.28)	0.15

a) Energies are in kJ mol^{-1} with ZPE and without ZPE in parenthesis. b) Numerical values of BD in this table are expressed as the population relative to the global minima of 1.0. c) Using the B3LYP/6-31G(d) geometries. d) From Ref. 14.

previous studies[23] that emphasized the good performance of the B3LYP/6-31G(d) method but with a tendency to overestimate the energetic importance of the intramolecular hydrogen-bonded interactions.

In all of the dyes except for AA, the planar conformations (MS3 type), which are not listed in the table, are calculated to be in high relative energies at the B3LYP/6-31+G(d) level: 13.1, 20.9, 25.4, and 25.7 kJ mol^{-1} (without ZPE corrections) for BA, PA, IA, and CA, respectively. The conformers listed in Table 2 have low enough energies to be significantly populated but are highly dependent on the acyl groups. In the cases of IA and PA, the global minimum conformations are major contributors to the Boltzmann distributions, whereas the other dyes investigated have two or three low-energy conformations, indicating high flexibility in their geometries. It is noted that the energy difference in CA between the rotamers of the acyl R group (MS1 and MS1r) is rather small, yet the *cis* isomer (MS1), in which the cyclopropyl group lies cis with respect to the carbonyl group, is favorable in agreement with a previous study[24] on cyclopropanecarboxylic acid. According to the study[24] based on the picture of the Walsh model,[25] the π-conjugation between the quasi-π orbital of the cyclopropane ring and the π-orbital of the carbonyl group reaches its maxima at cis and trans forms, and the *cis* isomer is a little favorable due to steric effects; the energy difference between cis and trans of cyclopropanecarboxylic acid has been calculated to be 4.14 kJ mol^{-1} at B3LYP/6-311++G(d,p) level with ZPE corrections.[24]

Absorption Spectra. Figure 5 shows the measured absorption spectra in a visible region of the dyes in ethyl acetate, and

Table 3 indicates the numerical values of the peak wavelengths and their molar extinction coefficients (ε_{max}). The spectra for BA and PA are almost consistent with those reported[14] for the corresponding dyes without ballast groups, and in all cases the peaks in the visible region are located around 435 nm, resulting in a yellow color. Noticeably, observed molar extinction coefficients (ε_{max}) vary by 1.5 times, depending on the acyl groups, without a significant shifting in the main peak wavelengths. To the best of our knowledge, IA shows the highest molar extinction coefficient among the yellow 2-acylacetanilide azomethine dyes reported to date. Another interesting result is the distinct increase of absorption by changing the acyl group from open- (PA) to closed-ring (CA). Figure 5 also shows the difference of the spectrum curves in the long-wavelength tail extending into the green region, demonstrating the degree of absorption in the green region on the order of IA ≤ CA < PA < BA ≤ AA. Table 3 also gives the absorption wavelengths and oscillator strengths (f_{calc}) calculated for the lower energy transitions using the global and local minimum structures. As listed in Table 3, the observed absorption wavelengths for the dyes are reproduced quantitatively by the TD-DFT calculations with the global minimum geometries, though unfortunately diffuse functions do not improve them; the mean absolute and maximum errors in calculated excitation energies for the main peaks are 0.03 and 0.07 eV, respectively, for the 6-31G(d) basis set and 0.04 and 0.08 eV, respectively, for the 6-31+G(d) basis set. In these results, the basis set with an additional set of diffuse functions tends to give systematically smaller transition energies than those without them; the mean and maximum energy differences between the two basis sets are 0.05 and 0.05 eV, respectively. It should be noted that the errors in calculated excitation energies mentioned above are rather small when compared to those known in previous reports on the other types of dyes; those values known often amount to 0.2 eV.[12]

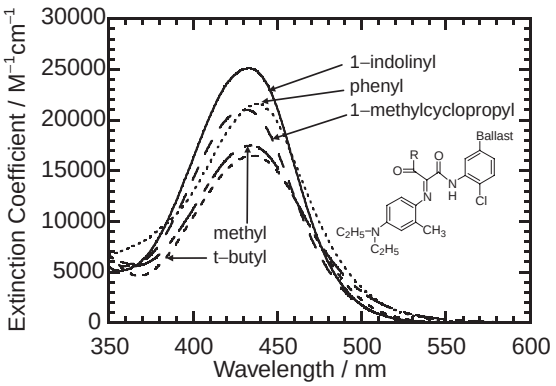

Fig. 5. Measured spectra of the dyes investigated in ethyl acetate (25 °C). Approximately 1 mM solutions in 1 mm cells.

To compare calculated and experimental oscillator strengths directly, the experimental values (f_{exp}) were determined from experimental absorption coefficients using the relation:[26]

$$f_{exp} \cong 4.319 \times 10^{-9} \varepsilon_{max} \Delta\omega, \quad (1)$$

where ε_{max} is the measured molar extinction coefficient in

Table 3. Calculated and Experimental Absorption Wavelengths and Oscillator Strengths

		B3LYP/6-31G(d)			B3LYP/6-31+G(d)			Exptl	
Compd	Geometry	λ_{max} [a]	f_{calc} [a]	$f_{calc\text{-}sum}$ [b]	λ_{max} [a]	f_{calc} [a]	$f_{calc\text{-}sum}$ [b]	λ_{max}	f_{exp} (ε_{max})[c]
BA[d]									
	MS1	448.7	0.003	0.464	463.3	0.002	0.502	438	0.416(21600)
		429.9	0.445		437.5	0.473			
	MS2	444.1	0.292		459.1	0.247			
		402.3	0.204		415.3	0.297			
PA[d]									
	MS1	435.5	0.391	0.389	442.2	0.422	0.419	436	0.314(16470)
	MS2	456.5	0.351		466.1	0.376			
IA									
	MS1	422.9	0.496	0.524	429.8	0.524	0.537	433	0.442(25120)
	MS2	417.8	0.561		426.6	0.609			
		403.4	0.068		404.5	0.038			
CA									
	MS1	428.9	0.434	0.440	436.3	0.464	0.472	431	0.378(21040)
	MS1r	425.8	0.420		432.2	0.459			
	MS2	429.0	0.472		438.0	0.506			
AA									
	MS1	439.7	0.431	0.384	447.1	0.463	0.440	434	0.336(17500)
	MS2	446.0	0.415		456.4	0.452			
	MS3	514.7	0.278		521.4	0.317			
		417.3	0.241		417.8	0.249			

a) Wavelengths (λ_{max}/nm) and oscillator strengths calculated at each level using the B3LYP/6-31G(d) optimized structures. b) Boltzmann-weighted oscillator strengths calculated at each level (see text). c) Experimental oscillator strengths derived from Eq. 1 (see text). Molar extinction coefficients in parenthesis are measured for the ethyl acetate solution of 1×10^{-3} M. d) Wavelengths and oscillator strengths calculated at the B3LYP/6-31G(d) level are taken from Ref. 14.

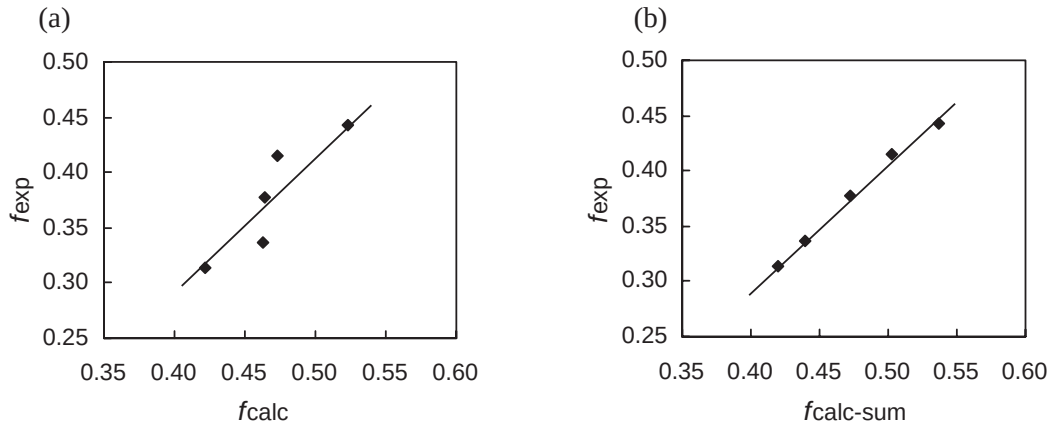

Fig. 6. Correlation of the experimental oscillator strength with that calculated at the B3LYP/6-31+G(d) level for the dyes investigated (see text): (a) f_{exp} vs f_{calc}, and (b) f_{exp} vs $f_{calc\text{-}sum}$.

L mol^{-1} cm^{-1}, and $\Delta\omega$ corresponds to the measured full-width at half-maximum of the absorption band in cm^{-1}. The values obtained from Eq. 1 neglect the solvent refractive index correction that may result in a systematic change.

The molecule in solution may exist in several conformations, which are located in global and local minima. Hence, the oscillator strengths (f_{calc}) for the peaks in the range of 400–500 nm calculated for global and local minima were weighted by the Boltzmann distribution derived from the relative energies with ZPE corrections (see Table 2), leading to the oscillator strengths ($f_{calc\text{-}sum}$) comparable to experimental values (f_{exp}). Those calculated results are collected in Table 3. Least-squares fits between the calculated and experimental values give linear correlation relationships and correlation coefficients (r):

$$f_{exp} = 1.309 f_{calc} - 0.237 \quad ; r = 0.892, \tag{a}$$
(f_{calc} was calculated with the 6-31+G(d) basis set)

$$f_{exp} = 1.126 f_{calc\text{-}sum} - 0.157 \quad ; r = 0.997, \tag{b}$$
($f_{calc\text{-}sum}$ was derived from f_{calc} and ΔE that were calculated with the 6-31+G(d) basis set)

$$f_{exp} = 1.288 f_{calc} - 0.188 \quad ; r = 0.908, \tag{c}$$
(f_{calc} was calculated with the 6-31G(d) basis set)

$$f_{exp} = 0.893 f_{calc\text{-}sum} - 0.016 \quad ; r = 0.965. \tag{d}$$
($f_{calc\text{-}sum}$ was derived from f_{calc} and ΔE that were calculated with the 6-31G(d) basis set)

Figure 6 shows the plots of (a) f_{exp} vs f_{calc} and (b) f_{exp} vs $f_{calc\text{-}sum}$, corresponding to Eqs. (a) and (b), respectively. Thus, the linear relationship in the Eq. (b) (Fig. 6b) provides a dramatic improvement in correlation coefficient, slope, and intercept when compared to those in the Eq. (a) (Fig. 6a); a similar improvement in those can be seen from Eqs. (c) to (d). Though the difference between experimental (f_{exp}) and calculated ($f_{calc\text{-}sum}$) values is significant as such, the trend of absorption intensities in the scope of 2-acylacetanilide azomethine dyes is well reproduced by the relation in Eq. (b) or (d). In other words, it was confirmed that the absorption spectra for the dyes are represented by the superposition of the transitions derived from the global and local minima coexisting in equilibrium.

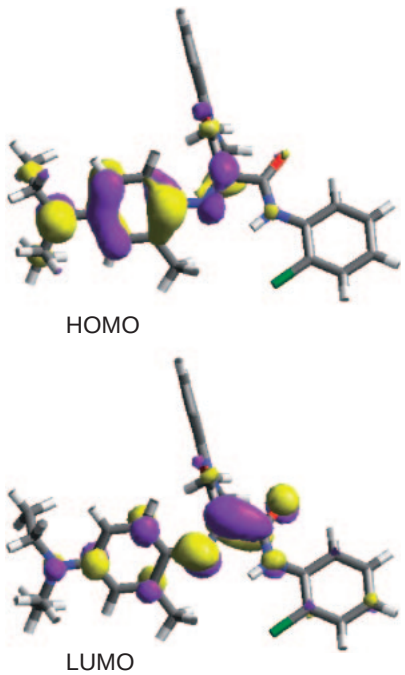

Fig. 7. Frontier molecular orbitals for IA in the global minimum (MS1) obtained by B3LYP/6-31G(d) level.

Discussion

Electronic Transition Properties. Table 4 indicates the main configurations for the lower energy transitions obtained by the TD-DFT calculations. The main transitions for the main peaks are primarily assigned to the π–π^* type transitions corresponding to those from HOMO (highest occupied molecular orbital) to LUMO (lowest unoccupied molecular orbital). For example, Figure 7 shows the frontier molecular orbitals obtained for IA in the global minimum (MS1). HOMO mainly delocalizes in the *p*-aminophenyl–azomethine fragment and LUMO in *p*-aminophenyl–azomethine–carbamoyl fragment.

Table 5 shows the numerical values of the HOMO, LUMO, HOMO–LUMO gap ($\Delta\varepsilon$), and excitation energies calculated for the main peaks by the TD-DFT method. In the case of

Table 4. Main Configuration and Its Weight for the Lower Energy Transitions[a)]

Compd	Geometry	B3LYP/6-31G(d) Configuration (weight %)	B3LYP/6-31+G(d) Configuration (weight %)
BA			
	MS1	H → L + 1[b)] (46)	H → L + 1[b)] (47)
		H → L (37)	H → L (38)
	MS2	H → L (35), H → L + 1[b)] (6.5)	H → L (35), H → L + 1[b)] (8.6)
		H → L + 1[b)] (40)	H → L + 1[b)] (38)
PA			
	MS1	H → L (38)	H → L (39)
	MS2	H → L (37)	H → L (38)
IA			
	MS1	H → L (38)	H → L (39)
	MS2	H → L (36)	H → L (38)
		H − 1[c)] → L (46)	H − 1[c)] → L (48)
CA			
	MS1	H → L (38)	H → L (39)
	MS1r	H → L (37), H − 2[d)] → L (5.5)	H → L (38)
	MS2	H → L (36), H − 2[d)] → L (5.3)	H → L (38)
AA			
	MS1	H → L (37)	H → L (38)
	MS2	H → L (35), H − 2[d)] → L (6.3)	H → L (37)
	MS3	H → L (29), H − 2[d)] → L (10)	H → L (31), H − 2[d)] → L (8.8)
		H − 1[e)] → L (37), H − 2[d)] → L (6.3)	H − 1[e)] → L (36), H − 2[d)] → L (7.7)

a) Only configurations with the weight over 5% are shown in the table. H and L denote HOMO and LUMO, respectively. b) Benzoyl π orbital. c) Indolinylcarbonyl fragment π orbital. d) Imino N lone-pair, acyl O π, cyclopropane quasi-π, and carbamoyl O lone-pair orbitals. e) *N*-Phenylcarbamoyl fragment π orbital.

Table 5. Calculated HOMO Energy, LUMO Energy, HOMO–LUMO Energy Gap ($\Delta\varepsilon$), and Excitation Energy[a)]

Compd	Geometry	B3LYP/6-31G(d) HOMO	LUMO	$\Delta\varepsilon$	Excitation[b)]	B3LYP/6-31+G(d) HOMO	LUMO	$\Delta\varepsilon$	Excitation[b)]
BA									
	MS1	−5.09	−1.81	3.28	2.88	−5.34	−2.12	3.22	2.83
	MS2	−5.12	−1.92	3.20	2.79	−5.37	−2.24	3.13	2.70
PA									
	MS1	−5.14	−1.87	3.27	2.85	−5.39	−2.17	3.22	2.80
	MS2	−5.12	−1.97	3.16	2.72	−5.37	−2.27	3.10	2.66
IA									
	MS1	−5.14	−1.85	3.29	2.93	−5.39	−2.16	3.24	2.88
	MS2	−5.19	−1.92	3.26	2.97	−5.43	−2.23	3.20	2.91
CA									
	MS1	−5.09	−1.80	3.28	2.89	−5.34	−2.11	3.23	2.84
	MS1r	−5.14	−1.83	3.31	2.91	−5.40	−2.14	3.26	2.87
	MS2	−5.12	−1.87	3.25	2.89	−5.37	−2.18	3.19	2.83
AA									
	MS1	−5.12	−1.91	3.21	2.82	−5.38	−2.23	3.15	2.77
	MS2	−5.15	−1.99	3.16	2.78	−5.41	−2.31	3.09	2.72
	MS3	−5.13	−2.32	2.80	2.41	−5.38	−2.63	2.76	2.38

a) Energies are in eV. b) Calculated for main absorption transitions by TD-DFT method. Correspond to the calculated main peak wavelengths (λ_{max}) in Table 3.

MS3 for AA, both the $\Delta\varepsilon$ and excitation energies are relatively small due to the planar conformation and the hydrogen bond. These structural features are largely different from the other conformations, and MS3 is not included in the following analysis. A plot of the excitation energies versus $\Delta\varepsilon$ at 6-31+G(d) level is shown in Fig. 8, indicating that the excitation energies, on the whole, depend on $\Delta\varepsilon$. It concurs with the result that the main peak is dominated by the singly excited configuration HOMO → LUMO (see Table 4). The slope larger than unity in Fig. 8 suggests that the exchange integral[26b] increases with increasing $\Delta\varepsilon$. Namely, the overlapping between HOMO and LUMO more delocalizes with increasing $\Delta\varepsilon$. This is mainly because as the twisting of t5 proceeds, HOMO localizes on the *p*-aminophenyl group and LUMO on the azo-

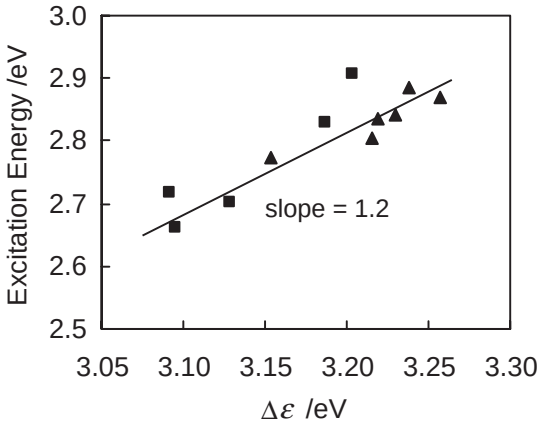

Fig. 8. Plot of excitation energy for main transition versus HOMO–LUMO energy gap ($\Delta\varepsilon$) calculated for MS1 (triangles) and MS2 (squares) types of conformations at B3LYP/6-31+G(d) level.

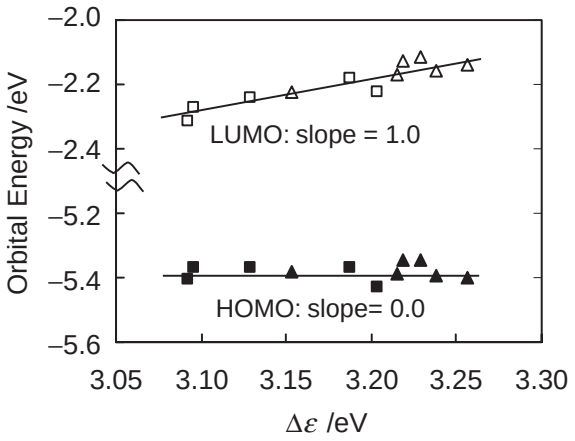

Fig. 9. Plots of HOMO and LUMO energies versus HOMO–LUMO energy gap ($\Delta\varepsilon$) calculated for MS1 (triangles) and MS2 (squares) types of conformations at B3LYP/6-31+G(d) level.

methine–carbamoyl fragment. Thus, the large slope shown in Fig. 8 is due to the change in the separation of electron distributions between HOMO and LUMO, the excitation being of charge-transfer character with increasing deviations of t5 from 0°. In contrast, a similar plot for the small molecules in which such a separation does not occur is shown to have a slope of 0.86 in the literature[27] by the same calculation method with the same basis set as our present study.

To illustrate the influence that the HOMO and LUMO energies have on $\Delta\varepsilon$, they are plotted separately versus $\Delta\varepsilon$ in Fig. 9. It is shown that nearly all of the variation in $\Delta\varepsilon$ occurs from changes in the LUMO, not HOMO energies. It is also noteworthy from Table 5 and Fig. 9 that the LUMO energies for MS1 of the dyes are higher than those for MS2, and the variation in those for MS1 is relatively small. The reason is that the acyl groups in MS1, of which t6 are calculated to be around 90°, exert inductive effects through σ-bonds whereas those in MS2, of which t6 are largely deviated from 90°, exert inductive and mesomeric effects. The inductive effect of the acyl groups has an influence on both the HOMO and LUMO energies simultaneously, whereas the mesomeric effect of the acyl groups has an electron-withdrawing influence on the LUMO energy due to the large LUMO coefficient on the azomethine carbon atom. For this reason, the observed absorption wavelengths hardly vary depending on acyl groups, since they are well reproduced by the TD-DFT calculations using MS1 conformations, of which t6 are calculated to be around 90°.

The lowering of the LUMO energies of MS2 for IA and CA is, however, not so large when compared to those for the other dyes. It is because of the less electron-withdrawing nature of these acyl groups due to electron-donating 1-indolinyl and 1-methylcyclopropyl groups. This nature of the cyclopropyl group is known to be due to the three-center, doubly-degenerated, occupied π-orbitals (the Walsh orbitals).[28] It is also known from classical theory that when compared to the *tert*-butyl group, the cyclopropyl group is equivalent in Hammett constant σ_p but more electron-donating in Swain–Lupton resonance parameter R.[29]

Despite the lowering of $\Delta\varepsilon$ energies from MS1 to MS2, the excitation energies of MS2 in the cases of IA and CA become high or nearly equivalent (see Table 5). It is due to their high planarity of t5, which results in the increase of exchange integral. Consequently, because of both electronic effects and the planarity of t5, the differences in main peak wavelengths calculated for IA and CA between global and local minima are very small unlike the cases in the other dyes, explaining their sharp-cut curves of spectra observed in the long-wavelength sides.

The variation in HOMO energies of all of the dyes is small and not systematic for the changing of deviations of t5 from 0°, despite the out-of-phase combination between N7 and C8 in the *p*-aminophenyl–azomethine fragment (see Fig. 7); for example, HOMO as well as LUMO energies of MS1 for IA and PA are calculated to be almost equal (see Table 5) despite the largest difference in t5 for MS1 among the dyes. However, a change of excitation energies by the TD-DFT method between them amounts to 0.08 eV (at 6-31+G* level in Table 5). These results indicate that deviations of t5 from 0° calculated for the dyes cause the separation of electron distributions between the HOMO and LUMO, but are not so large to induce changing the HOMO as well as LUMO energies.

Absorption Intensities vs Structural Features. The experimental intensity (f_{exp}) of the dye increases on the order of IA > BA ≥ CA > AA > PA, which is fairly consistent with the order of decreasing deviations of t5 from 0° for MS1 and MS2: IA < CA = BA < AA < PA. Although the observed ε_{max} varies by 1.5 times from PA to IA, it includes the difference of shapes between their spectrum curves, which is mainly due to the differences of intensities among the conformers and of their Boltzmann distributions. When considering the systematic error between calculated and observed values (see Fig. 6b), the intensity ratio of IA to PA is calculated to be 1.4 for MS1. The difference in the absorption intensities is because of the overlap density between the occupied and unoccupied MOs associated with the transition. We have already discussed that the large deviations of t5 from 0° result in the decrease of overlapping between HOMO and LUMO. Thus, the observed absorption intensities strongly depend on

the deviations of t5 from 0° for the highly populated conformers.

The simultaneous deviations of t5 and t6 from 0° and 90° often occur because of the mutual steric crowding among *p*-aminophenyl, acyl, and carbamoyl fragments. In addition, the two π-conjugative interactions of *p*-aminophenyl– and acyl–azomethine fragments compete for stabilization. Thus, the twisting of t5 and t6 is a result of the delicate balance between steric and electronic effects, but the deviations of t5 seem to be governed mainly by steric rather than electronic factors. As shown in Fig. 4, the steric repulsion in MS1 occurs between R and methyl, and that in MS2 between R and C9H. The high planarity of the t5 calculated for IA suggests the influence of the shape of the acyl group, of which characteristic features are the planar, rigid, and properly bulky ring system. A comparison between PA and CA can be interpreted as that between spherical sizes open- and closed-ring acyl R isomers; the change from PA to CA results in a decrease of the steric repulsions mentioned above in MS1 and MS2. To compare the sizes of substituents in the molecules, the steric substituent parameters (the STERIMOL parameters) calculated based on the van der Waals radius of atoms are known.[30] The changing of isopropyl to cyclopropyl groups reduces the parameters with respect to the longest length of them from 3.16 to 2.88.[30]

On the other hand, we consider that the electronic effects of acyl groups may partly affect the planarity of t5. A possibility of σ–π orbital interactions[31] can be considered. They are the σ–π^* orbital interaction between the σ-orbital for the R–carbonyl bond in the acyl group and the π^*-orbital for the azomethine bond, and vice versa. The evidence for such orbital interactions is indicated in the slightly large $\Delta\varepsilon$ energies for MS1 (and MS1r) of IA and CA compared to those of the others. It is because the σ–π^* interaction destabilizes the LUMO and the σ^*–π interaction stabilizes the HOMO, though we cannot apparently recognize such an orbital mixing in the picture of the frontier orbitals. However, these interactions occur to MS1 in the spatial relation between the acyl group and the azomethine fragment, which is mutually orthogonal, and weakly occur to MS2, which is twisted from orthogonality. Therefore, these interactions are not dominant factors for the planarity of t5, since for IA and CA the planarity of t5 in MS2 is higher than that in MS1. Electronic effects appear to be weak also in the reported results for both nitro and amino substituents at the *p*-position of benzoyl group, which exhibit almost similar absorption intensities (ε_{max}) as well as maxima (λ_{max}).[2]

The above discussions on steric effects are also related to the relative energy of MS2. The steric repulsion between acyl R and carbamoyl groups as well as that between acyl R and *p*-aminophenyl groups occurs at the large twisting of t6 for MS2, and it is assumed to increase with increasing bulkiness of acyl R group. Therefore, the relative energy calculated for MS2 increases on the order of PA > IA > CA > BA. In the case of AA, due to having the smallest acyl group among the dyes, torsion angle t6 can deviate largely from 90° to extend π-conjugation of the *p*-aminophenyl–azomethine fragment into the acetyl group. This π-conjugative interaction leads to the relatively large twisting of t5 and to the large relative energy of MS2, in disagreement with the order of increasing bulkiness of the acyl R group.

Conclusion

The relationship between visual absorption properties and molecular structures was investigated on a series of yellow azomethine dyes derived from 4-diethylamino-2-methylaniline and 2-acyl-2′-chloroacetanilides. Three types of conformational isomers in common for the dyes were obtained by DFT calculations: two of them were MS1 and MS2 types, which are attributed to deviations from planarity of *p*-aminophenyl–azomethine fragments, and the other was the nearly planar MS3 type.

Observed electronic absorption wavelengths were well reproduced by TD-DFT calculations at global minimum geometries (MS1). The calculated excitation energies for the main peaks, on the whole, depend on the HOMO–LUMO energy gap ($\Delta\varepsilon$). The acyl groups nearly perpendicular to the azomethine fragment in global minima exert weak inductive effects, and their variation slightly altered frontier orbital energies while leaving the $\Delta\varepsilon$ almost unchanged. These calculated results explain the nearly equal peak wavelengths observed for the dyes.

For IA and CA, the main peak wavelengths calculated for global and local minima were very close unlike the cases in the other dyes, explaining the sharp-cut curves of spectra observed in the long-wavelength sides. The marked red shifts calculated for MS2 of BA, AA, and PA are due to the large deviations of t6 from 90°, which cause a lowering of the LUMO energies by electron-withdrawing (mesomeric) effects of acyl groups. In the case of MS2 for IA and CA, the acyl groups are less electron withdrawing because of the electron-donating acyl R groups. In addition, the relatively high planarity of t5 in MS2 for IA and CA raises the excitation energies more than expected from their $\Delta\varepsilon$.

Absorption intensities observed for the dyes investigated vary by 1.5 times from minimum to maximum, demonstrating the largest absorption of IA and the distinct increase of absorption by changing the acyl group from open- (PA) to closed-ring (CA). The linear-squares fit between the calculated and experimental oscillator strengths gives a good linear correlation relationship when the calculated oscillator strengths are weighted by the Boltzmann distribution. The experimental oscillator strength (f_{exp}) of the dye increases fairly consistently with the order of decreasing deviations of t5 from 0° for MS1 and MS2. The large deviations of t5 from 0° cause the separation of the electron distributions between HOMO and LUMO, resulting in the decrease of overlapping between them. The deviations of t5 seem to be governed mainly by steric rather than electronic factors. IA among the dyes is calculated to be the smallest deviations of t5, suggesting that it is because of the planar, rigid, and properly bulky ring system of the acyl group. A comparison between PA and CA can be interpreted as that between spherical sizes open- and closed-ring acyl isomers, accounting for the smaller deviations of t5 from 0° for CA than for PA.

References

1 For review articles: a) R. D. Theys and G. Sosnovsky, *Chem. Rev.*, **97**, 83 (1997). b) P. Bergthaller, *Imaging Sci. J.*, **187**, 50 (2002). c) R. Bradbury, "Advances in Color Chemistry

Series 3, (Modern Colorants: Synthesis and Structures)," Blackie A & P, Glasgow (1995), pp. 154–155.

2 G. H. Brown, J. Figueras, R. J. Gledhill, C. J. Kibler, F. C. McRossen, S. M. Parmerter, P. W. Vittum, and A. Weissberger, *J. Am. Chem. Soc.*, **79**, 2919 (1957).

3 M. Adachi, Y. Murata, and S. Nakamura, *J. Am. Chem. Soc.*, **115**, 4331 (1993).

4 M. J. S. Dewar, E. G. Zoebisch, E. F. Healy, and J. J. P. Stewart, *J. Am. Chem. Soc.*, **107**, 3902 (1985).

5 a) J. E. Ridley and M. C. Zerner, *Theor. Chim. Acta*, **32**, 111 (1973). b) A. D. Bacon and M. C. Zerner, *Theor. Chim. Acta*, **53**, 21 (1979). c) M. C. Zerner, G. H. Loew, R. F. Kirchner, and U. T. Mueller-Westerhoff, *J. Am. Chem. Soc.*, **102**, 589 (1980).

6 L. E. Friedrich and J. E. Eilers, *J. Imaging Sci. Technol.*, **38**, 24 (1994).

7 a) N. Saito and S. Ichijima, The International Symposium on Silver Halide Imaging (1997). b) H. Kobayashi, K. Yamada, Y. Yoshioka, H. Fukunaga, S. Ichijima, and K. Ogawa, The International Congress of Photographic Science Meeting, Belgium (1998).

8 S. Daiba, T. Oshiyama, and F. Ishii, *J. Soc. Photogr. Sci. Technol. Jpn.*, **62**, 371 (1999).

9 F. Abu-Hasanayn and W. G. Herkstroeter, *J. Phys. Chem. A*, **105**, 1214 (2001).

10 a) P. Hohenberg and W. Kohn, *Phys. Rev.*, **136**, B864 (1964). b) W. Kohn and L. J. Sham, *Phys. Rev.*, **140**, A1133 (1965). c) R. G. Parr and W. Yang, "Density-Functional Theory of Atoms and Molecules," Oxford University Press, Oxford (1989).

11 a) R. Bauernschmitt and R. Ahlrichs, *Chem. Phys. Lett.*, **256**, 454 (1996). b) M. E. Casida, C. Jamorski, K. C. Casida, and D. R. Salahub, *J. Chem. Phys.*, **108**, 4439 (1998). c) C. Jamorski, M. E. Casida, and D. R. Salahub, *J. Chem. Phys.*, **104**, 5134 (1996).

12 a) C. Muguruma, N. Koga, Y. Hatanaka, I. El-Sayed, M. Mikami, and M. Tanaka, *J. Phys. Chem. A*, **104**, 4928 (2000). b) J. Danielsson, J. Ulin, and A. Laaksonen, *J. Am. Chem. Soc.*, **123**, 9817 (2001). c) J. L. Weisman and M. H. Gordon, *J. Am. Chem. Soc.*, **123**, 11686 (2001). d) R. Bauernschmitt, R. Ahlrichs, F. H. Hennrich, and M. M. Kappes, *J. Am. Chem. Soc.*, **120**, 5052 (1998). e) D. Guillaumont and S. Nakamura, *Dyes Pigm.*, **46**, 85 (2000).

13 a) T. Z. Ando, *Phys. B*, **26**, 263 (1977). b) A. Zangwill and P. Soven, *Phys. Rev. A*, **21**, 1561 (1980). c) E. Runge and E. K. U. Gross, *Phys. Rev. Lett.*, **52**, 997 (1984).

14 S. Ichijima, H. Fukunaga, H. Kobayashi, M. Ishihara, and N. Koga, *Bull. Chem. Soc. Jpn.*, **76**, 733 (2003).

15 a) M. Motoki, S. Ichijima, N. Saito, T. Kamio, and K. Mihayashi, (Fuji Photo Film Co., Ltd., Japan), U. S. Patent 5213958 (1993). b) M. Motoki, N. Saito, T. Kamio, M. Tanaka, and S. Ichijima, (Fuji Photo Film Co., Ltd., Japan), U. S. Patent 5214141 (1993).

16 Y. Shimura, H. Kobayashi, and Y. Yoshioka, (Fuji Photo Film Co., Ltd., Japan), U. S. Patent 5427902 (1995).

17 Y. Shibahara, K. Yamada, and S. Ishimaru, *Fujifilm Res. Dev.*, **40**, 1 (1995).

18 A. D. Becke, *J. Chem. Phys.*, **98**, 1372 (1993).

19 C. Lee, W. Yang, and R. G. Parr, *Phys. Rev. B*, **37**, 785 (1988).

20 A. D. Becke, *J. Chem. Phys.*, **98**, 5648 (1993).

21 A. P. Scott and L. Radom, *J. Phys. Chem.*, **100**, 16502 (1996).

22 M. J. Frisch, G. W. Trucks, H. B. Schlegel, G. E. Scuseria, M. A. Robb, J. R. Cheeseman, V. G. Zakrzewski, J. A. Montgomery, Jr., R. E. Stratmann, J. C. Burant, S. Dapprich, J. M. Millam, A. D. Daniels, K. N. Kudin, M. C. Strain, O. Farkas, J. Tomasi, V. Barone, M. Cossi, R. Cammi, B. Mennucci, C. Pomelli, C. Adamo, S. Clifford, J. Ochterski, G. A. Petersson, P. Y. Ayala, Q. Cui, K. Morokuma, D. K. Malick, A. D. Rabuck, K. Raghavachari, J. B. Foresman, J. Cioslowski, J. V. Ortiz, A. G. Baboul, B. B. Stefanov, G. Liu, A. Liashenko, P. Piskorz, I. Komaromi, R. Gomperts, R. L. Martin, D. J. Fox, T. Keith, M. A. Al-Laham, C. Y. Peng, A. Nanayakkara, M. Challacombe, P. M. W. Gill, B. Johnson, W. Chen, M. W. Wong, J. L. Andres, C. Gonzalez, M. Head-Gordon, E. S. Replogle, and J. A. Pople, "Gaussian 98, Revision A.7," Gaussian Inc., Pittsburgh, PA (1998).

23 a) C. S. Callam, S. J. Singer, T. L. Lowary, and C. M. Hadad, *J. Am. Chem. Soc.*, **123**, 11743 (2001). b) M. T. Gordon, T. L. Lowary, and C. M. Hadad, *J. Org. Chem.*, **65**, 4954 (2000).

24 X.-J. Hou and M.-B. Huang, *J. Mol. Struct.: THEOCHEM*, **585**, 93 (2002).

25 A. D. Walsh, *Trans. Faraday Soc.*, **45**, 179 (1949).

26 For review articles: a) J. G. Calvert and J. N. Pitts, Jr., "Photochemistry," John Wiley and Sons Inc., New York (1966), p. 172. b) M. Klessinger and J. Michl, "Excited States and Photochemistry of Organic Molecules," VCH Publishers, Inc., New York (1995), pp. 11–21.

27 C.-G. Zhan, J. A. Nichols, and D. A. Dixon, *J. Phys. Chem. A*, **107**, 4184 (2003).

28 For example: R. Wolfgang, "The Chemistry of the Cyclopropyl Group," ed by Z. Rappoport, John Wiley and Sons Inc., New York (1987), pp. 57, 61, 62.

29 For a survey of Hammett substituent constants and resonance parameters: a) C. Hansch, A. Leo, and R. W. Taft, *Chem. Rev.*, **91**, 165 (1991). b) C. Hansch, A. Leo, S. H. Unger, K.-H. Kim, D. Nikaitani, and E. J. Lien, *J. Med. Chem.*, **16**, 1207 (1973).

30 A. Verloop, W. Hoogenstraaten, and J. Tipker, "Drug Design, VII," ed by E. J. Ariëns, Academic Press, New York (1976), pp. 175–180.

31 For a review article: R. Gleiter and L. A. Paquette, *Acc. Chem. Res.*, **16**, 328 (1983).